Supplementary Information

for

Fewer temperature ties: scalable integration and broad selection of phase change materials for both heating and cooling

Xiaoxue Kou [1], Jiatong Jiang [1], Baoshan Xie [1], He Shan [1], Primož Poredoš [1,2], Ruzhu Wang [1, *]

1 Institute of Refrigeration and Cryogenics, MOE Engineering Research Center of Solar Power and Refrigeration, Shanghai Jiao Tong University, Shanghai 200240, China

2 Laboratory for Sustainable Technologies in Buildings, Faculty of Mechanical Engineering, University of Ljubljana, Ljubljana, Slovenia

*Corresponding author: rzwang@sjtu.edu.cn

Note 1. Heat pump model

To critically evaluate and optimize the system performance, a detailed heat pump model is developed under these fundamental assumptions:

(1) The heat pump operates in a steady state;

(2) Gravitational and kinetic energy are negligible, along with minor pressure drop in heat exchangers;

(3) The refrigerant is assigned a superheat of 4.5°C in the evaporator and a subcooling of 2.5°C in the condenser.

The relationship between the supplied heat/cold thermal energy and the ambient can be determined once equilibrium occurs between the thermal energy provision power and the heat dissipation power amidst the enclosed space and its surrounding atmosphere. The details are shown in Fig. S1.
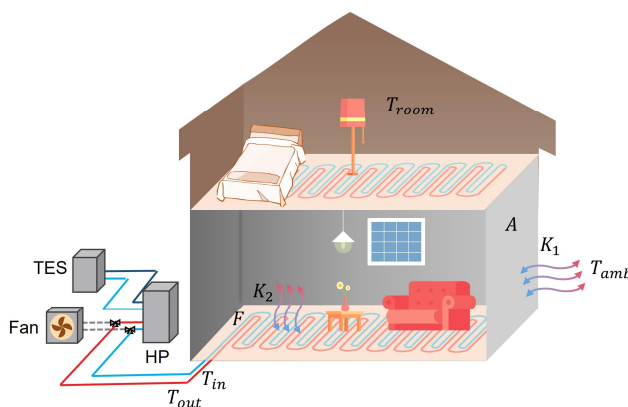

Figure S1. Thermal equilibrium model within a house

$$\dot{Q}_{hs} = AK_1\left(T_{room} - T_{amb,w}\right) = FK_2\left(\frac{T_{hs,in} + T_{hs,out}}{2} - T_{room}\right) \tag{1}$$

$$\dot{Q}_{cs} = AK_1\left(T_{amb,s} - T_{room}\right) = FK_2\left(T_{room} - \frac{T_{cs,in} + T_{cs,out}}{2}\right) \tag{2}$$

where, the left part represents the heat dissipation power and the right part is the thermal energy

supply power, symbolized by $\dot{Q}_{hs}$ and $\dot{Q}_{cs}$. $T_{amb,w}$ $T_{amb,s}$ denote the ambient temperatures in winter and summer. $T_{hs,in}$ and $T_{cs,in}$ are the heat and cold supply temperature, and correspondingly, $T_{hs,out}$ and $T_{cs,out}$ are the return temperature of heat and cold supply. The supply and return temperatures are set with a 20 ℃ differential. A is the surface area of the building's enclosed structure, and K_1 refers to the heat transfer coefficient of the enclosed structure. The indoor temperature, designated as T_{room}, is assumed to be 22 ℃. F is the heat transfer area of the indoor heat exchanger, and K_2 represents the heat transfer coefficient.

R134a is opted for in this study due to its compatibility with the two-stage operation temperature range of heat pumps. The heat absorbed by the refrigerant in the evaporator $q_{abs'}$ or $q_{abs''}$ (1'→2' and 1"→2") is:

$$q_{abs'(abs'')} = h_{2'(2'')} - h_{1'(1'')} \tag{3}$$

where h is the specific enthalpy of the refrigerant, and the superscript $'$ and $''$ represent the first and second stages of heat pump cycles.

The electrical input by the positive-displacement compressor $p_{cmp'}$ or $p_{cmp''}$ is:

$$p_{cmp'(cmp'')} = \frac{h\left(p_{3'(3'')}, s_{2'(2'')}\right) - h_{2'(2'')}}{\eta_{is}\eta_v\eta_{el}\eta_{me}} \tag{4}$$

where, the isentropic efficiency η_{is}, volumetric efficiency η_v, electricity efficiency η_{el}, mechanical efficiency η_{me} are maintained at 0.85, 0.85, 0.97, 0.98 [1], respectively.

The heat released by the refrigerant in the condenser $q_{rel'}$ or $q_{rel''}$ (3'→4' and 3"→4") is:

$$q_{rel'(rel'')} = h_{3'(3'')} - h_{4'(4'')} \tag{5}$$

Within a heat pump cycle, the refrigerant mass flow rate is determined by the heat/cold thermal energy charging and discharging power and the thermal energy demands from users:

$$\dot{m}_{ref,h'} = \dot{m}_{ref,h''} \frac{q_{abs''}\tau_{discharge,h}}{q_{rel'}\tau_{charge,h}} \tag{6}$$

$$\dot{m}_{ref,h''} = \frac{\dot{Q}_{hs}}{q_{rel''}} \tag{7}$$

$$\dot{m}_{ref,c'} = \dot{m}_{ref,c''} \frac{q_{rel''}\tau_{discharge,c}}{q_{abs'}\tau_{charge,c}} \tag{8}$$

$$\dot{m}_{ref,c''} = \frac{\dot{Q}_{cs}}{q_{abs''}} \tag{9}$$

where $\dot{m}_{ref'}$, $\dot{m}_{ref''}$ are the refrigerant mass flow rates of the first and second heat pump cycles. $\tau_{discharge}$ and τ_{charge} denote the duration of the charging and discharging processes. The subscripts h and c stand for heating and cooling, respectively.

Note 2. Heat pumps and intermediate PCMs coupling model

Regarding heat pumps and intermediate PCMs coupling model, the underlying assumptions are as follows:
(1) Phase change materials maintain a continuous uniform temperature throughout their melting and solidifying processes;

(2) The model assumes no heat and temperature loss of thermal energy in storage stages;

The stored heat/cold thermal energy in the intermediate storage unit encompasses both latent and sensible parts.

$$Q_{str,h(c)} = m_{PCM,h(c)} \left(\int_{T_{min}}^{T_{pc}} c_{p,s} \, dT + h_{latent} + \int_{T_{pc}}^{T_{max}} c_{p,l} \, dT \right) \tag{10}$$

$$m_{PCM} = \max\left(m_{PCM,h}, m_{PCM,c}\right) \tag{11}$$

where, $m_{PCM,h(c)}$ signifies the required mass of phase change materials to adequately deliver in-time heating or cooling power to end-users within a specified period $\tau_{discharge}$. The actual mass of phase change material contained within the storage unit m_{PCM} is the upper limit of the targeted phase change material mass, namely $m_{PCM,h}$ and $m_{PCM,c}$. $m_{PCM,h}$ and $m_{PCM,c}$ retain their pivotal role in quantifying the stored thermal energy of charging and discharging operations related to heat and cold provision. T_{min} and T_{max} are assumed as $T_{pc} - 2$ and $T_{pc} + 2$ to ensure the latent heat is fully utilized.

A shell-and-tube heat exchanger facilitates the interaction between the refrigerant and phase change materials as depicted in Fig. S2. This simplified model represents the one-dimensional heat transfer among these substances. The refrigerant flows along the inner walls of the tubes, while phase change materials undergo a phase change process outside the tubes.
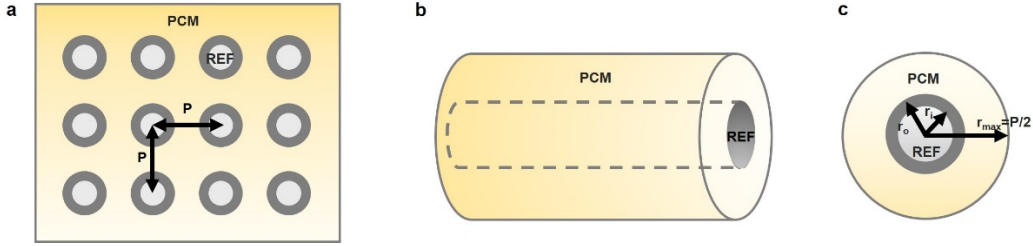

Figure S2. Physical model of shell-and-tube latent thermal energy storage unit. (a) 2D schematic diagram. (b) Simplified 1D model. (c) Parameters of simplified 1D model.

The heat transfer process in the steady state between phase change materials and the refrigerant is:

$$\dot{m}_{ref} \Delta h_{ref} = \frac{\Delta T}{R_{ex} + R_{ref} + R_{PCM}} \tag{12}$$

where, $\dot{m}_{ref}$ is the mass flow rate of refrigerant, and Δh_{ref} is the specific enthalpy difference between refrigerant input and output. The heat transfer temperature difference between the refrigerant and phase change materials, designated as ΔT, delineates the phase change temperature difference between the refrigerant and phase change materials. The denominator of the right-side term includes the thermal resistance of the heat exchanger tube R_{ex}, the refrigerant R_{ref}, and the phase change materials R_{PCM} [2].

$$R_{ex} = \frac{\ln\left(\frac{r_o}{r_i}\right)}{2\pi k_{ex} L_{ex}} \tag{13}$$

where, r_o, r_i and k_{ex} are the outer radius, inner radius, and thermal conductivity of the heat

exchanger tube, respectively. The length of one set of heat exchanger tubes, designated as L_{ex}, is calculated according to m_{PCM} and the number of sets of heat exchange tubes n_{set} (n_{set} varies between 4 and 6 to limit $L_{ex}<L_{max}$).

To augment the heat transfer between phase change materials and heat transfer fluid, these materials are customarily constrained within a limited spatial region, accommodating compact fins or strategically inserting metal foams [3]. Consequently, the convection within phase change materials throughout the melting and solidification processes is negligible, permitting the heat transfer within phase change materials to be estimated by thermal conduction [4,5]. The thermal resistance of phase change materials can subsequently be estimated [2], with the attributes of the applicable heat exchanger [2,6].

$$R_{PCM} = \frac{\ln\left(\frac{(\delta(r_{max}^2 - r_o^2) + r_o^2)^{\frac{1}{2}}}{r_o}\right)}{2\pi L_{ex} k_{PCM,id}} \tag{14}$$

where, δ is the fraction of phase change materials that has yet to change the phase during the phase change process. An average estimation of this value is conservatively set at 0.5. r_{max} refers to the maximum distance in which the phase change front from one tube meets the phase change front of another tube, which equals half of the pitch distance P [2]. $k_{PCM,id}$ signifies the ideal thermal conductivity of PCMs.

$$R_{ref} = \frac{1}{h_0 A_{ex}} \tag{15}$$

where, A_{ex} is the heat transfer area of the refrigerant, and h_0 denotes the average convective coefficient of the refrigerant in tubes.

While the occurrence of refrigerant boiling inside the tubes poses a more intricate process, it is noted that refrigerant forms stratified flow within horizontal tubes under scenarios of low mass flux (<50 kg/m²·s) and low heat flux (<2 kW/m²) [7]. The Liu and Winterton correlation is invoked here to calculate the convective heat transfer coefficient h_0 for in-tube evaporation, as delineated in eqn (16-20) [8]. For the estimation of in-tube condensation, the optimized expression employed is the Shah correlation (eqn (21)), which predicts the mean convective heat transfer coefficient associated with condensation across the range of vapor quality from 1 to 0 [9].

$$h_{evp} = ((Eh_{cb})^2 + (Sh_{nb})^2)^{0.5} \tag{16}$$

$$h_{cb} = 0.023 Re_l^{0.8} Pr_l^{0.4} \frac{k_l}{D_i} \tag{17}$$

$$h_{nb} = 55 p_r^{0.12} \left(-log_{10}(p_r)\right)^{-0.55} M^{-0.5} \frac{\dot{m}_{ref}}{\pi r_i^2}^{0.67} \tag{18}$$

$$E = \left(1 + xPr_l \left(\frac{\rho_l}{\rho_v} - 1\right)\right)^{0.35} \tag{19}$$

$$S = \frac{1}{1 + 0.055 E^{0.1} Re_l^{0.16}} \tag{20}$$

where, p_r is contrast pressure; Pr_l is Prandtl number; Re_l is Reynolds number; M is the relative

molecular mass of the refrigerant. $\dot{m}_{ref}$ is the mass flux, and x denotes vapor quality. ρ_l and ρ_v are the density of liquid and gaseous refrigerants. k_l is the thermal conductivity of liquid refrigerant, and D_i is the inner diameter of heat exchange tubes.

$$h_{cond} = h_L \left(0.55 + \frac{2.09}{p_r^{0.38}} \right) \tag{21}$$

where, h_L is the convective heat transfer coefficient, assuming all the mass flow as liquid, and is calculated by the Dittus-Boelter equation.

Note 3. Model validation

Validation of the heat pump model with the refrigerant of R134a is achieved through the experiment data acquired from our previous study on the single-stage operation of a scroll compressor heat pump [10]. Comprehensive operational details pertaining to this heat pump are provided in Table S1. A comparison between the simulation and experimental coefficient of performance (COP) can be found illustrated in Fig. S3. The model validity under varying operating conditions is ensured by examining the COP at varied evaporation and condensation temperatures, T_{evap} and T_{cond}. The COP prediction agrees well with experimental values, deviating by less than 5%. This confirms the suitability of the heat pump model for further study.

Table S1. Detailed information about the operation of the actual heat pump [10]

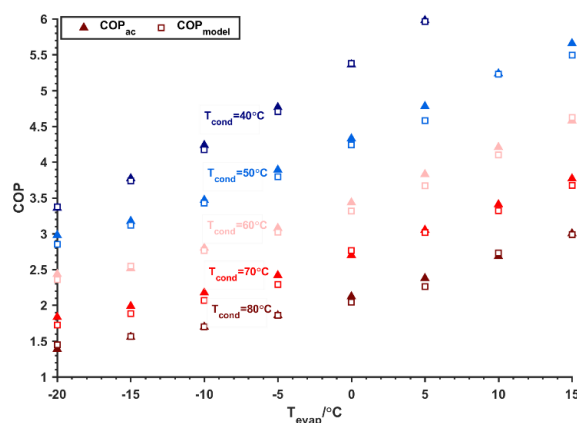| Parameters	Value
Refrigerant	R134a
Displacement of the compressor	60 cm^3/rev
Rated speed of the motor	4500 rmp
Evaporator and Condenser	Shell and tube heat exchanger
Tube length/inside diameter of heat exchangers	5750/19 mm
Number of tubes	2

Figure S3. The comparison of the simulation and experimental results [10]

The comprehensive analysis and verification of the thermal resistance within the latent thermal energy storage unit, including phase change material and heat exchanger thermal resistance, is executed following our previous extensive experimental and simulation examination on a three-

dimensional latent thermal energy storage unit [11,12]. Figure S4 delineates the structural data of the 3D latent thermal energy storage unit. The precise thermal resistance is determined using the heat transfer power and temperature differential between the heat transfer medium water and the phase transition material PCM 90. The previously developed 3D numerical model effectively simulates the temperature fluctuations of phase change materials during charging and discharging. Consequently, the thermal resistance within the latent thermal energy storage unit derived from integrating the numerical model and experimental findings is compared with that derived via the simplified methodology employed in this paper. The values of the two are 256.195 K/W and 246.732 K/W, respectively. The deviation of the model used in this paper does not exceed 4%.
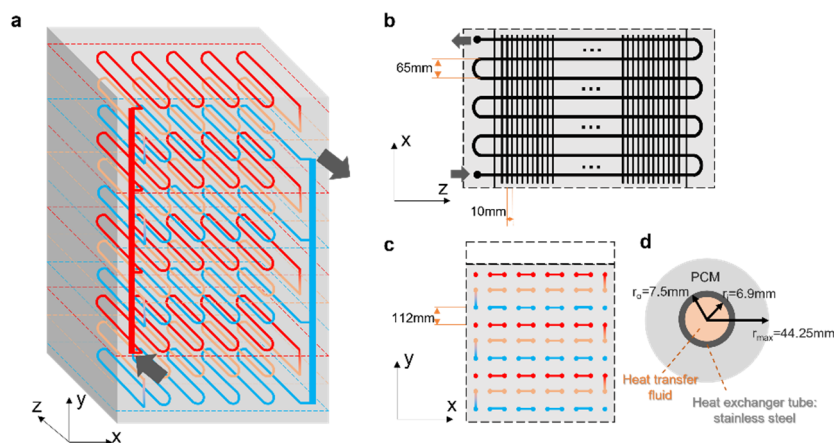
Figure S4. Structure information of the three-dimensional latent thermal energy storage unit [11,12]

The heat pump and latent thermal energy storage coupling model is substantiated via existing researches [13,14]. Detailed structural data and thermophysical attributes of phase change materials and the refrigerant are tabulated in Table S2. Paraffin, exhibiting a phase change temperature range of 40-44°C, serves as a verification subject, given that the integration of heat pumps and phase change materials with a phase transition temperature band of 10.5~22°C remains unexplored to its full potential and lacks comprehensive investigation. In order to verify the validity of the refrigerant and phase change material coupling model, we have performed a theoretical analysis on the heat storage power and compared it against the data gathered in the literature [13]. Fig. S5 presents the correlation between the predicted heat storage power and the PCM-side condensation temperature ranging from 54.7°C to 56.4°C alongside the air-side evaporation temperature of -26°C. While charged, the phase change material within the two-phase region gradually elevates temperature, accordingly increasing the condensation temperature of the heat pump. During this stage, the charging power displays a declining trend in fluctuations. The comparison between the results of our heat pump and latent thermal energy storage coupling model and the reference [13] reveals an average discrepancy of 7.71%, indicating an accurate prediction of the coupled heat transfer process.

Table S2. Detailed structure information and thermal properties of phase change materials and the refrigerant during heat transfer process [13]

Parameters		Value
Heat storage unit	Tube length per row	6 m
	Row number	16

	Outer radius of the heat exchanger tube	5 mm
	Inner radius of the heat exchanger tube	4 mm
	Heat exchanger tube	Copper
	Pinch distance of the heat exchanger tube	200 mm
	Phase change temperature	40-44°C
	Thermal conductivity coefficient	0.2 W/m·K⁻¹
Heat pump	Refrigerant	R410a
	Compressor displacement	34 m³/h
	Isentropic exponent of R410A	1.16
	Evaporation temperature	-26°C
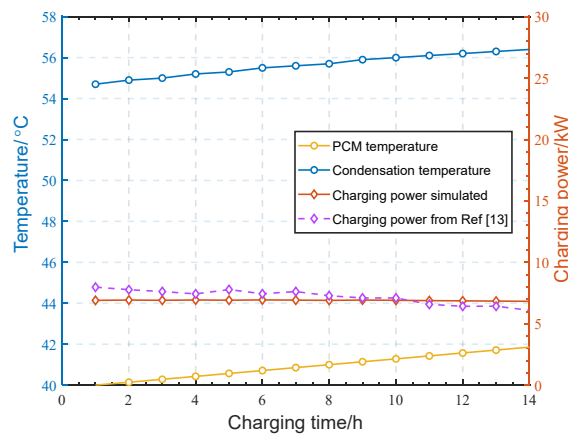
Figure S5. The comparison of charging power between the simulation and results from Ref. [13]

Based upon evaluation, validated mathematical models are utilized to thoroughly scrutinize operating characteristics and performance of the intermediate thermal energy storage system.

Note 4. Characterization of phase change materials

The properties of phase change materials fundamentally determine the configuration and operating conditions of the heat pump, alongside the whole system. Within this context, the focus is primarily directed toward the phase change temperature, latent heat of phase transition, specific heat capacity, and thermal conductivity, as well as the density of intermediate thermal energy storage materials as illustrated in Fig. S6.
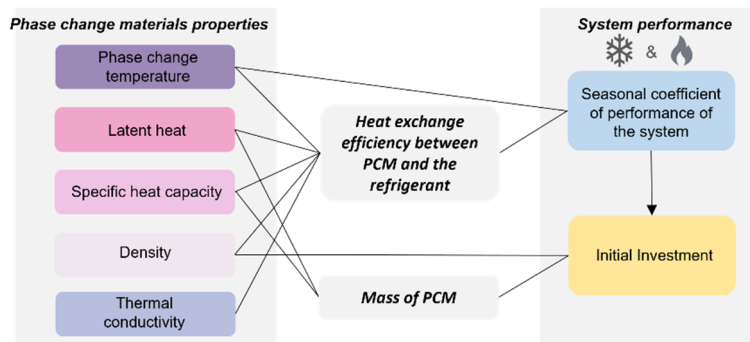
Figure S6. Thermophysical properties of phase change materials and their interconnection with

the system performance

The phase change temperature has an impact on the evaporation or condensation temperatures of four heat pump cycles for heating and cooling, consequently influencing the COP of heat pump cycles. The annual coefficient of performance of the intermediate thermal energy storage system is optimized by adjusting the temperature difference of the first and second heat pump cycles within an established temperature range between heat/cold supply temperatures and ambient temperatures. Moreover, fluctuations in refrigerant evaporation and condensation temperatures directly impact the convective heat transfer coefficient of the refrigerant, thereby affecting heat exchange performance. Both the Liu and Winterton correlation and Shah correlation underscore this point, indicating that evaporation and condensation temperatures alter refrigerant's thermal properties such as density, viscosity, specific heat capacity and enthalpy of phase transition, as well as thermal conductivity.

The latent heat and specific heat capacity serve as pivotal determinants in the mass of materials to store specific amounts of thermal energy according to eqn. (10). Along with density, these inherent characteristics impact the determination of the volume of contained phase change materials and the required heat transfer area. Given a predetermined heat transfer area, the geometry of the heat exchanger impacts the thermal resistance of the refrigerant and heat exchanger tube as demonstrated by eqn. (13)-(15). This secondary influence on the heat exchange efficiency dictates the heat exchange temperature difference between phase change materials and the refrigerant. It further modulates the annual coefficient of performance of the system. Moreover, alterations in the phase change materials mass and required heat transfer area of the heat exchanger affect the upfront capital expenditure of the intermediate thermal energy storage system.

Recognized as one of the underlying impediments to the mainstream adoption of thermal storage materials, enhancing the thermal conductivity of phase change materials is crucial. An undesirable low thermal conductivity significantly decelerates the energy charging and discharging processes. If the thermal conductivity of a substance is heightened, heat can be disseminated more swiftly within the substance, allotting a diminutive temperature difference between the fluid and the substance. Hence, thermal conductivity significantly affects the heat exchange efficiency between the phase change materials and the refrigerant, further impacting the steady-state heat transfer temperature difference between the storage unit and heat pumps, consequently impacting the evaporation or condensation temperature of heat pump cycles, thereby affecting the COP and the overall system performance.

Note 5. High-throughput screening of phase change materials

Within the intermediate temperature band, numerous phase change materials are accessible. Nonetheless, the feasibility of materials is mainly determined by the phase change temperature and thermal conductivity enhancement degree defined by eqn (25). Targeting at the intermediate both heat and cold thermal energy storage and catering to the operation of the heat pump, a margin of T_s is established between the storage temperature of phase change materials and the ambient temperature in winter or summer [15]. Specifically, intermediate both heat and cold thermal energy storage mandates a moderate temperature differential between the storage temperature and ambient

in winter and summer. Moreover, to prevent near thresholds for evaporation and condensation of heat pumps, an operational allowance T_s is stipulated. Upon meeting the phase change temperature criteria $T_{amb,w} + T_s < T_{pc} < T_{amb,s} - T_s$, the material is validated as eligible and progresses to subsequent layers. This step serves to signify their potential application within an intermediate thermal energy storage mechanism.

Regarding potential phase change materials in the next layer, their application necessitates thermal conductivity enhancement as the majority of phase change materials exhibit inferior thermal conductivity, typically below 0.5 W/(m·K). The extent of thermal conductivity enhancement M_k ranges from 1.5 to 120 times with the inclusion of carbon-based or metal-based addictive [3]. As such, given a predetermined steady-state heat transfer temperature difference, the required thermal conductivity enhancement degree is specified in eqn (25). Limited by the current thermal conductivity enhancement measures, M_k has to be less than $M_{k,max}$ (assumed as 120 [3]). Once the requisite improved thermal conductivity ensures technological feasibility for thermal conductivity enhancement, i.e., $M_k < M_{k,max}$, it is qualified for subsequent layers.

$$M_k = \frac{k_{PCM,id}}{k_{PCM,ac}} \tag{25}$$

where, $k_{PCM,ac}$ is the actual thermal conductivity of phase change material candidates, $k_{PCM,id}$ is the requisite thermal conductivity with a predetermined steady-state heat transfer temperature difference.

The third layer pivots around the PCM-specified unit design to ascertain the viability of system functioning. The volume of storage phase change materials determines the required heat exchange area of heat exchanger tubes, specifically, the number of sets of heat exchanger tubes n_{set} and the length of one set of heat exchanger tubes. Herein, the feasibility of unit design is primarily dictated by its tube length. With maximum n_{set}, the longest single-group tube length is assumed as L_{max} (assumed as 6m here [16]), as tubes with excessive length exacerbate temperature distribution unevenness within the storage unit. Moreover, it also leads to an extended latent-sensible heat exchange stage when the refrigerant flows through the heat exchanger tube, thereby degrading the performance of the heat exchange process. In addition, given a maximum number of groups, if the length of one set of heat exchanger tubes remains greater than L_{max}, it will result in a significant increase in the cost of the storage unit, as the expenditure on heat exchangers constitutes a hefty share of the overall latent thermal energy storage cost [16,17].

After confirming the feasibility of both materials and unit design, the subsequent two layers are primarily applied to evaluate prospective materials that exhibit superior energy and economic performance (detailed in Note S6).

Note 6. Performance metrics of the TES system

The identification of performance indicators for this system is predominantly in line with the inherent energy and economic advantages, encompassing annual coefficient of performance and investment cost, as well as annual net income. These metrics particularly underscore their implications for energy consumption and cost efficacy.

The annual coefficient of performance of this system η takes into account the coefficient of performance in the heating case η_h and coefficient of performance in the cooling case η_c. The thermal energy exchanged with the ambient, either as output or input energy, is not incorporated within eqn (23) and (24), as it is perceived to be freely attainable. Consequently, the annual coefficient of performance of the system remains consistently comparable with the coefficient of performance (COP) of heat pumps.

$$\eta = \eta_h \omega_h + \eta_c \omega_c \tag{22}$$

$$\eta_h = \frac{Q_{hs}}{W' + W''} \tag{23}$$

$$\eta_c = \frac{Q_{cs}}{W' + W''} \tag{24}$$

where, ω_h and ω_c signify the ratio of heating days and cooling days to total number of thermal energy supply days. Q_{hs} and Q_{cs} refer to the daily heat and cold thermal energy consumption of users. W' and W'' are the electricity consumed by the first and second stages of heat pump cycle.

Eqn (25) elucidates the investment costs C_0 attributed to the integrated system.

$$C_0 = C_{com} + C_{txv} + C_{ex} + C_{TES} + C_{ref} \tag{25}$$

where, C_{com} is in unity with the acquisition costs of the compressor, encompassing both main body of the compressor and the electric motor. C_{txv} represents the cost of the expansion valve, and C_{ex} is the cost of heat exchangers functioning either as evaporators or condensers. C_{TES} pertains to the purchased cost of the latent thermal energy storage unit, comprising the cost of phase change materials along with their containment, ignoring the dead volume of the storage unit. The cost associated with shell and tube heat exchanger C_{ex} can be obtained from Ref. [18,19].

$$C_{com} = a_1 k_1 \left(\frac{V}{0.9 - \eta_{is}}\right)\left(\frac{P_{3(3')}}{P_{2(2')}}\right)\left(\ln \frac{P_{3(3')}}{P_{2(2')}}\right) + a_2 k_2 p_e \left(\frac{\eta_{el}}{1 - \eta_{el}}\right) \tag{26}$$

$$C_{txv} = a_3 k_3 m_r \tag{27}$$

$$C_{ex} = a_4 k_4 m_w \sqrt{\frac{\eta_{eva(con)}}{1 - \eta_{eva(con)}}} \tag{28}$$

$$C_{TES} = a_5 (c_{PCM} m_{PCM} + C_{ex}) \tag{29}$$

where, a_m is the annuity factor for the m-th component, following $a_m = \frac{i}{1-(1+i)^{-n_m}}$. i is an annual nominal interest rate, and n_m signifies the depreciation time of the m-th component. k_m refers to the cost coefficient of the components [20].

In scenarios where specific material prices are either concealed or not publicly available due to commercial confidentiality, inferences can be made based on computations involving recognized phase change materials, which exhibit similar characteristics and properties.

CF_{net} represents the annual cost benefits of the system, precisely determined by deducting operating expenses, including electrical power expenditure, from the income earned through heating and refrigeration production.

$$CF_{net} = K_{h\&c} Y_{h\&c} - K_{el} Y_{el} \tag{30}$$

where, $K_{h\&c}$ is the price of heat/cold thermal energy generated through electricity, and K_{el} refers to the electricity cost when the heat pump operates to realize thermal energy provision. $Y_{h\&c}$ signifies the daily heating and refrigeration production. Y_{el} denotes electricity consumption.

Note 7. Separate heat and cold storage system
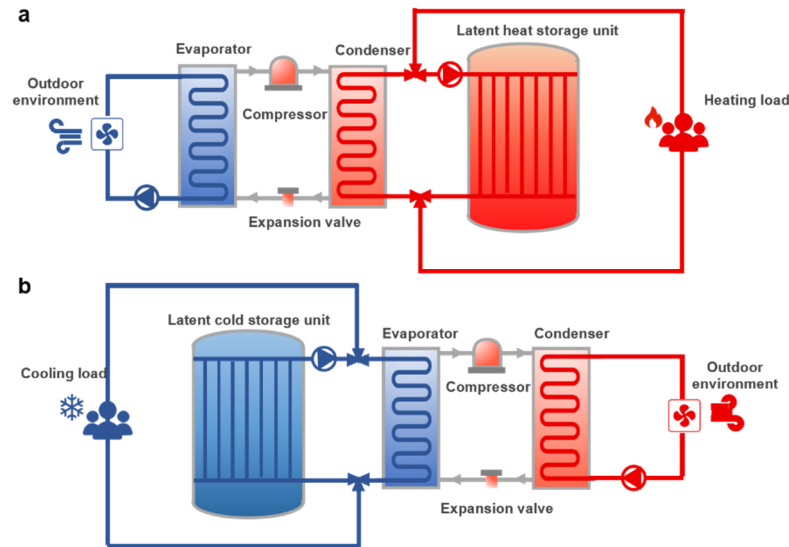
Figure S7 Scheme of the separate heat and cold storage system: (a) conventional integration system for heating, (b) conventional integration system for cooling

The separate heat and cold storage system serves as one of the main comparison objects due to its substantial cost savings under time-of-use tariffs via thermal energy storage, as well as its compatibility with conventional heat pump systems.

In separate heat and cold storage systems, the heat pump is integrated with two separate heat and cold storage units in winter and summer, respectively. In winter, the condenser of an air-source heat pump is connected to a latent heat storage unit with a specific storage temperature, and the user is supplied with heat by the storage unit. In summer, the evaporator of the air-source heat pump is integrated with a latent cold storage unit with a specific storage temperature, and the user is supplied with cold by the storage unit.

Table S3. Phase change materials database for intermediate thermal energy storage

No.	Materials	Phase change temperature/°C	Latent heat/J·g⁻¹	Thermal conductivity /W·m⁻¹·K⁻¹	Specific heat capacity (l) /kJ·kg⁻¹·K⁻¹	Specific heat capacity (s) /kJ·kg⁻¹·K⁻¹	Density /kg·m⁻³	Cost /$·kg⁻¹	Reference
1	RT10	10	165	0.2	2	2	825	42.22*	[21]
2	RT10 HC	10	200	0.2	2	2	825	50.67*	[21]
3	S10	10	170	0.43	1.9	1.9	1470	25.14*	[22]
4	A10	10	210	0.22	2.16	2.16	770	25.14*	[22]
5	SP9_gel	10.5	155	0.6	2	2	1350	42.22*	[21]
6	Isopropyl palmitate	11	98	0.24	1.78	1.78	852	25*	[23,24]
7	RT11HC	11	200	0.2	2	2	825	50.67*	[21]
8	A11	11	210	0.22	2.16	2.16	775	25.14*	[22]
9	RT12	12	165	0.2	2	2	825	42.22*	[21]
10	A12	12	215	0.22	2.16	2.16	775	25.14*	[22]
11	Pelargonic acid	12.3	127	0.129	1.87	1.866	869.9	0.9-10.6	[25,26]
12	SP11_gel	12.5	155	0.6	2	2	1325	42.22*	[21]
13	S13	13	150	0.43	1.9	1.9	1515	25.14*	[22]
14	A13	13	225	0.22	2.16	2.16	775	25.14*	[22]
15	A14	14	200	0.22	2.16	2.16	775	25.14*	[22]
16	RT15	15	155	0.2	2	2	825	42.22*	[21]
17	S15	15	180	0.43	1.9	1.9	1510	25.14*	[22]
18	A15	15	205	0.18	2.16	2.16	780	25.14*	[22]
19	A16	16	225	0.18	2.16	2.16	780	25.14*	[22]
20	SP15_gel	16	160	0.6	2	2	1350	42.22*	[21]
21	Caprylic acid	16	149	0.145	2.13	1.46	921.5	3.5-120	[26–28]
	Acetic acid	16.7	184	0.18	2.04	2.04	1050	0.40-1.20	[26,29]
23	S17	17	155	0.43	1.9	1.9	1525	25.14*	[22]
24	A17	17	235	0.18	2.18	2.18	780	25.14*	[22]
25	Dodecanol	17.5	203	0.14	2.44	2.44	831	119.3*	[23,30]
26	PCM RT18	16-19	134	0.2	2	2	756	42.22*	[31]
27	Hexadecane paraffin	18	236	0.085	2.1	1.65	780	1.0-20.0	[26,32]
28	RT18HC	18	260	0.2	2	2	825	50.67*	[21]
29	S18	18	145	0.43	1.9	1.9	1520	25.14*	[22]
30	A18	18	155	0.22	2.18	2.18	765	25.14*	[22]
31	Glycerin/Glycerol	18.1	199	0.292	1.25	1.251	1291	1.6*	[25]
32	PCM-EP (Propyl Palmitate/Expanded Perlite-Based Form-Stable Composite)	18.5	82	0.125	1.9	1.6	559.5		[33]
33	KF·4H₂O	18.5	231	0.48	1.84	1.84	1437	0.88-1.00	[23,24,26]

34	Butyl stearate	19	140	0.14	0.46	0.46	861	24[*]	[23,24]
35	S19	19	175	0.43	1.9	1.9	1520	25.14[*]	[22]
36	A19	19	150	0.22	2.18	2.18	765	25.14[*]	[22]
37	S20	20	195	0.54	2.2	2.2	1530	25.14[*]	[22]
38	A20	20	160	0.22	2.2	2.2	770	25.14[*]	[22]
39	RT21	21	165	0.2	2	2	825	42.22[*]	[21]
40	RT21HC	21	190	0.2	2	2	825	50.67[*]	[21]
41	S21	21	220	0.54	2.2	2.2	1530	25.14[*]	[22]
42	A21	21	160	0.22	2.2	2.2	770	25.14[*]	[22]
43	8% wt. Expanded graphite nanosheets 92% wt. Paraffin, nheptadecane ($C_{17}H_{36}$)	21.1	26.2	0.419	2.24	2.312	658.5	8.16[*]	[34]
44	n-Heptadecane	22	215	0.21	1.99	1.992	778	1.0-15.0	[25,26]
45	RT22	22	200	0.2	2	2	825	42.22[*]	[35]
46	RT22HC	22	190	0.2	2	2	730	50.67[*]	[21]
47	S22	22	215	0.54	2.2	2.2	1530	25.14[*]	[22]
48	A22	22	160	0.18	2.2	2.2	785	25.14[*]	[22]
49	SP21EK	22	170	0.5	2	2	1550	42.22[*]	[21]
50	Natural TCM energy saver	18-26	179	0.375	1.79	1.785	1300	2.11[*]	[36]
51	Paraffin(22°C)	22	165	0.1	2.8	2.8	900	1.88-2.00	[37,38]
52	80% paraffin + 15% HDPE + 5% EG	17.03-26.97	148	0.2	2	2	825	2.22[*]	[39]
53	S23	23	200	0.54	2.2	2.2	1530	25.14[*]	[22]
54	A23	23	155	0.18	2.2	2.2	785	25.14[*]	[22]
55	RT25	23-25	160	0.2	3	3	820	42.22[*]	[40]
56	RT24HC	24	200	0.2	2	2	750	50.67[*]	[21]
57	S24	24	180	0.54	2.2	2.2	1530	25.14[*]	[22]
58	A24	24	155	0.18	2.22	2.22	790	25.14[*]	[22]
59	SP24E	24.5	180	0.5	2	2	1550	42.22[*]	[21]
60	RT25HC	25	230	0.2	2	2	825	50.67[*]	[21]
61	S25	25	175	0.54	2.2	2.2	1530	25.14[*]	[22]
62	A25	25	220	0.18	2.22	2.22	785	25.14[*]	[22]
63	SP25E2	25	180	0.5	2	2	1550	42.22[*]	[21]
64	DuPont Energain® M27 (biobased)	21,23,25,27,29	200	0.2	1.97	1.97	235	1.65-5.55	[41]
65	Bio-PCM Q23	25.5	70	0.157	0.84	0.837	801	2	[42]
66	SP-25 A8	25-26	180	0.6	2.5	2.5	1380	42.22[*]	[43]
67	Lauryl alcohol	25.83	216	0.144	2.32	2.322	890.9	1.85-100	[25,26]

68	A26	26	230	0.21	2.22	2.22	790	25.14*	[22]
69	SP26E	26	180	0.5	2	2	1550	42.22*	[21]
70	Micronal PCM®DS 5001 X	26	120	0.55	1.07	1.1	1248	4.31	[44]
71	CADE (mixture of capric acid+1-dodecanol)	26.1-26.5	127	0.16	2.08	1.89	785.5	15.55*	[45]
72		25-28	184	0.2	4.81	3.11	880		[46]
73	$Na_2HPO_4 \cdot 12H_2O$ - $K_2HPO_4 \cdot 3H_2O$ SiO_2	26.5	145.3	0.3	2.1	2.1	1000	3.33*	
74	RT25	26.6	232	0.185	1.8	1.41	767	42.22*	[47,48]
75	Paraffin RT27	26-28	179	0.2	2.4	1.8	810	42.22*	[43]
76	S27	27	185	0.54	2.2	2.2	1530	25.14*	[22]
77	A27	27	250	0.22	2.22	2.22	768	25.14*	[22]
78	RT27 paraffin + SBS	27	110	0.23	2.5	2.8	805.5	36.32*	[49]
79	GR27	27	64.9	0.2	1.92	2.044	1360	42.22*	[50,51]
80	Octadecane paraffin	28	244	0.26	2.1	1.75	780	1.0-20.0	[26,32]
81		27-29	205	0.21	2.23	2.23	850		[52]
82	RT28HC	28	250	0.2	2	2	825	50.67*	[21]
83	A28	28	265	0.21	2.22	2.22	789	25.14*	[22]
84	Paraffin(28.2°C)	28.2	245	0.25	2.2	1.934	794.5	1.88-2.00	[38,53]
85	A29	29	230	0.21	2.22	2.22	785	25.14*	[22]
86	In-organic	29	220	0.805	1.7	1.46	1260		[54]
87	Capric acid	29.3	162	0.265	2	2	941	1-100	[55]
88	$CaCl_2 \cdot 12H_2O$	29.8	174	0.81	1.4	2.2	1710	0.13-0.2	[38,56]
89	$CaCl_2 \cdot 6H_2O$	29.9	187	0.81	1.4	2.2	1682	0.1 - 0.19	[26,56,57]
90	A30	30	230	0.21	2.22	2.22	790	25.14*	[22]

*Quotations from commercial companies

Table S4. Main parameters in operations of the intermediate thermal energy storage system

	Parameters	Value
	Indoor room temperature	295.15 K
Operational parameters	Pinch temperature between HP and the ambient/users	5 K
	Charging period (τ_{charge})	8 h
	Discharging period ($\tau_{discharge}$)	5 h
Economic parameters	Annual nominal interest rate (i)	5%
	Depreciation time of components (n_m)	12 years [20]
	Cost coefficient of HP components (k_m)	6560, 0.09, 4621, 4621\$ [20]

Table S5. Parameters of heat pumps and thermal energy storage coupling model

	Parameters	Value
Geometric parameters	Outer radius of the heat exchanger tube (r_o)	5mm
	Inner radius of the heat exchanger tube (r_i)	4mm
	Pinch distance of the heat exchanger tube	70mm
Other parameters	Thermal conductivity of heat exchanger (k_{ex})	100 W/(m·K)
	Maximum temperature difference between PCM and refrigerant (ΔT)	3K
	Margin temperature between PCM and the ambient (T_s)	3K
	Surface area of the building enclosed structure (A)	125 m^2
	Heat transfer coefficient of the enclosed structure (K_1)	8 W/(m^2·K)
	Ratio of heat dissipation capacity of a dwelling to heat transfer capacity of a radiator (AK_1/FK_2)	1.5

Table S6. Advantageous phase change materials for specific countries/regions

Countries/regions	Advantageous phase change materials	Phase change temperature	Material type
Afghanistan	S21	21	Inorganic hydrated salt
Albania	SP15_gel	16	Inorganic macroencapsulated
Algeria	RT21HC	21	Organic
Argentina	A20	20	Organic
Armenia	S15	15	Inorganic hydrated salt
Azerbaijan	A16	16	Organic
Bhutan	Butyl stearate	19	Organic
Bosnia and Herzegovina	S15	15	Inorganic hydrated salt
Bulgaria	S15	15	Inorganic hydrated salt
Croatia	S15	15	Inorganic hydrated salt
Cyprus	RT18HC	18	Organic
Democratic People's Republic of Korea	SP15_gel	16	Inorganic macroencapsulated
France	Caprylic acid	16	Organic
Georgia	S15	15	Inorganic hydrated salt
Greece	A21	21	Organic
Hungary	A16	16	Organic
Iraq	n-Heptadecane	22	Organic paraffin
Islamic Republic of Iran	S21	21	Inorganic hydrated salt
Israel	A21	21	Organic
Italy	S20	20	Inorganic hydrated salt
Japan	S19	19	Inorganic hydrated salt
Jordan	A21	21	Organic
Kazakhstan	SP9_gel	10.5	Inorganic macroencapsulated
Korea	A17	17	Organic
Kuwait	RT21HC	21	Organic
Kyrgyzstan	SP15_gel	16	Inorganic macroencapsulated
Lebanon	S18	18	Inorganic hydrated salt
Malta	A21	21	Organic
Mongolia	SP15_gel	16	Inorganic macroencapsulated
Montenegro	S15	15	Inorganic hydrated salt
Morocco	A20	20	Organic
Nepal	S19	19	Inorganic hydrated salt
Norfolk Island	A19	19	Organic
Peru	A19	19	Organic

Plurinational State of Bolivia	RT18HC	18	Organic
Republic of Moldova	S13	13	Inorganic hydrated salt
Republic of North Macedonia	S15	15	Inorganic hydrated salt
Romania	S13	13	Inorganic hydrated salt
Serbia	S17	17	Inorganic hydrated salt
Slovenia	S15	15	Inorganic hydrated salt
Spain	S18	18	Inorganic hydrated salt
State of Palestine	A21	21	Organic
Swaziland	A17	17	Organic
Syrian Arab Republic	n-Heptadecane	22	Organic paraffin
Tajikistan	S21	21	Inorganic hydrated salt
Tunisia	A21	21	Organic
Turkey	Glycerin/Glycerol	18.1	Organic
Turkmenistan	S22	22	Inorganic hydrated salt
Ukraine	SP15_gel	16	Inorganic macroencapsulated
Uruguay	S18	18	Inorganic hydrated salt
Uzbekistan	S19	19	Inorganic hydrated salt

Table S7. Advantageous phase change materials for specific subnational states/ provinces/ autonomous regions

Subnational states/provinces/autonomous	Advantageous phase change materials	Phase change temperature	Material type
New South Wales	PCM RT18	17.5	Organic
South Australia	A18	18	Organic
Rio Grande do Sul	Dodecanol	17.5	Organic
Ontario	SP15_gel	16	Inorganic macroencapsulated
Anhui	S19	19	Inorganic hydrated salt
Beijing	Acetic acid	16.7	Organic
Chongqing	Natural TCM energy saver	22	Natural materials
Fujian	A22	22	Organic
Gansu	SP11_gel	12.5	Inorganic macroencapsulated
Guizhou	RT18HC	18	Organic
Henan	S19	19	Inorganic hydrated salt
Hubei	n-Heptadecane	22	Organic paraffin
Hebei	S20	20	Inorganic hydrated salt
Heilongjiang	S15	15	Inorganic hydrated salt
Hunan	n-Heptadecane	22	Organic paraffin
Jilin	S13	13	Inorganic hydrated salt
Jiangsu	Natural TCM energy saver	22	Natural materials
Jiangxi	n-Heptadecane	22	Organic paraffin
Liaoning	SP9_gel	10.5	Inorganic macroencapsulated
Nei Mongol	S15	15	Inorganic hydrated salt
Ningxia Hui	Acetic acid	16.7	Organic
Sichuan	RT21HC	21	Organic
Shandong	S20	20	Inorganic hydrated salt
Shanghai	Paraffin	22	Organic paraffin
Shaanxi	Acetic acid	16.7	Organic
Shanxi	SP11_gel	12.5	Inorganic macroencapsulated
Tianjin	S18	18	Inorganic hydrated salt
Xinjiang Uygur	S20	20	Inorganic hydrated salt
Yunnan	A20	20	Organic
Zhejiang	n-Heptadecane	22	Organic paraffin
Delhi	A21	21	Organic
Himachal Pradesh	RT21HC	21	Organic
Haryana	A21	21	Organic
Punjab	A21	21	Organic
Uttaranchal	RT21HC	21	Organic
Adygey	Acetic acid	16.7	Organic

Altay	S15	15	Inorganic hydrated salt
Astrakhan'	S18	18	Inorganic hydrated salt
Chechnya	Acetic acid	16.7	Organic
Dagestan	A13	13	Organic
Kabardin-Balkar	SP11_gel	12.5	Inorganic macroencapsulated
Krasnodar	Acetic acid	16.7	Organic
Kalmyk	SP15_gel	16	Inorganic macroencapsulated
Orenburg	S13	13	Inorganic hydrated salt
Rostov	Acetic acid	16.7	Organic
Samara	SP9_gel	10.5	Inorganic macroencapsulated
Saratov	SP9_gel	10.5	Inorganic macroencapsulated
North Ossetia	A13	13	Organic
Stavropol'	S13	13	Inorganic hydrated salt
Volgograd	S17	17	Inorganic hydrated salt
Alabama	RT18HC	18	Organic
Arkansas	n-Heptadecane	22	Organic paraffin
Arizona	n-Heptadecane	22	Organic paraffin
California	Butyl stearate	19	Organic
Colorado	SP11_gel	12.5	Inorganic macroencapsulated
Connecticut	S17	17	Inorganic hydrated salt
Delaware	Glycerin/Glycerol	18.1	Organic
Georgia	S15	15	Inorganic hydrated salt
Iowa	SP15_gel	16	Inorganic macroencapsulated
Idaho	S13	13	Inorganic hydrated salt
Illinois	Acetic acid	16.7	Organic
Indiana	Acetic acid	16.7	Organic
Kansas	Natural TCM energy saver	22	Natural materials
Kentucky	A17	17	Organic
Louisiana	Natural TCM energy saver	22	Natural materials
Massachussets	S17	17	Inorganic hydrated salt
Maryland	A17	17	Organic
Michigan	Acetic acid	16.7	Organic
Minnesota	S15	15	Inorganic hydrated salt
Missouri	Natural TCM energy saver	22	Natural materials
Mississippi	RT18HC	18	Organic
Montana	SP15_gel	16	Inorganic macroencapsulated
North Carolina	Dodecanol	17.5	Organic
North Dakota	SP9_gel	10.5	Inorganic macroencapsulated
Nebraska	S15	15	Inorganic hydrated salt
New Hampshire	Acetic acid	16.7	Organic

New Jersey	A17	17	Organic
New Mexico	S19	19	Inorganic hydrated salt
Nevada	Natural TCM energy saver	22	Natural materials
New York	S17	17	Inorganic hydrated salt
Ohio	A17	17	Organic
Oklahoma	Natural TCM energy saver	22	Natural materials
Oregon	A15	15	Organic
Pennsylvania	S17	17	Inorganic hydrated salt
Rhode Island	Acetic acid	16.7	Organic
South Carolina	Natural TCM energy saver	22	Natural materials
South Dakota	S17	17	Inorganic hydrated salt
Tennessee	S19	19	Inorganic hydrated salt
Texas	S17	17	Inorganic hydrated salt
Utah	SP11_gel	12.5	Inorganic macroencapsulated
Virginia	Dodecanol	17.5	Organic
Washington	A15	15	Organic
Wisconsin	S17	17	Inorganic hydrated salt
West Virginia	Acetic acid	16.7	Organic
Wyoming	SP15_gel	16	Inorganic macroencapsulated

Table S8. Detailed design and operation parameters of setups in specific countries/regions

Countries/regions	Mass of phase change materials/kg	Maximum refrigerant flow rate/m$^3\cdot$h^{-1}	Length of heat exchange tube in LTES/m	Sets of heat exchange tube in LTES
Afghanistan	102.53	43.73	5.93	3
Albania	114.78	32.16	5.64	4
Algeria	82.28	24.86	5.29	5
Argentina	91.20	23.49	5.24	6
Armenia	127.86	47.59	5.62	4
Azerbaijan	89.19	36.54	5.06	6
Bhutan	113.66	24.79	5.84	6
Bosnia and Herzegovina	114.60	38.60	5.03	4
Bulgaria	116.41	39.48	5.11	4
Croatia	110.84	36.60	4.87	4
Cyprus	52.56	21.17	5.63	3
Democratic People's Republic of Korea	149.54	51.37	5.88	5
France	124.54	32.65	5.97	6
Georgia	115.64	39.06	5.08	4
Greece	104.41	27.65	5.99	6
Hungary	94.69	40.06	5.37	6
Iraq	82.55	25.99	5.63	5
Islamic Republic of Iran	97.73	40.39	5.65	3
Israel	82.59	20.50	5.69	5
Italy	94.04	31.84	5.43	3
Japan	111.26	34.88	4.85	4
Jordan	99.79	26.03	5.73	6
Kazakhstan	159.60	62.49	5.23	6
Korea	92.86	41.81	5.26	6
Kuwait	103.17	21.33	5.53	6
Kyrgyzstan	145.42	48.49	5.71	5
Lebanon	111.64	27.06	4.87	4
Malta	73.11	17.61	5.04	5
Mongolia	171.83	75.02	5.63	6
Montenegro	109.74	36.04	4.82	4
Morocco	84.63	21.30	5.83	5
Nepal	89.53	25.63	5.21	3
Norfolk Island	62.56	13.77	5.42	4
Peru	69.24	15.54	4.80	5
Plurinational State of Bolivia	51.42	20.54	5.51	3
Republic of Moldova	146.40	45.00	5.13	5

Republic of North Macedonia	115.52	38.99	5.07	4
Romania	142.14	42.67	4.98	5
Serbia	135.49	39.38	5.89	4
Slovenia	114.83	38.72	5.04	4
Spain	108.62	25.91	4.74	4
State of Palestine	88.62	22.39	5.09	6
Swaziland	51.02	18.31	5.78	3
Syrian Arab Republic	82.92	30.14	5.65	5
Tajikistan	102.61	43.79	5.93	3
Tunisia	87.01	21.88	5.99	5
Turkey	101.61	36.56	5.22	4
Turkmenistan	100.26	40.42	5.79	3
Ukraine	144.48	47.88	5.68	5
Uruguay	97.25	22.65	5.66	3
Uzbekistan	124.56	42.09	5.43	4

Table S9. Detailed design and operation parameters of setups in specific subnational states/ provinces/ autonomous regions

Subnational states/provinces/autonomous	Mass of phase change materials/kg	Maximum refrigerant flow rate/m³·h⁻¹	Length of heat exchange tube in LTES/m	Sets of heat exchange tube in LTES
New South Wales	95.99	20.95	5.58	3
South Australia	91.74	21.57	5.30	6
Rio Grande do Sul	67.50	20.40	5.39	4
Ontario	161.03	47.44	5.27	6
Anhui	121.74	35.72	5.31	4
Beijing	140.2061	47.52	5.9033	6
Chongqing	101.92	28.52	5.20	4
Fujian	99.46	24.07	5.60	6
Gansu	155.56	44.40	5.19	6
Guizhou	73.36	30.05	5.90	4
Henan	126.57	37.54	5.52	4
Hubei	95.93	33.55	5.45	6
Hebei	130.85	46.57	5.67	4
Heilongjiang	177.65	69.71	5.20	6
Hunan	90.74	31.27	5.16	6
Jilin	197.09	62.52	5.75	6
Jiangsu	123.21	36.87	5.03	5
Jiangxi	88.56	30.24	5.03	6
Liaoning	170.82	52.79	5.59	6
Nei Mongol	165.79	60.93	5.82	5
Ningxia Hui	140.52	47.05	5.92	6
Sichuan	96.85	28.36	5.19	6
Shandong	121.73	41.37	5.28	4
Shanghai	118.2749238	32.76	5.8692	6
Shaanxi	123.62	39.03	5.20	6
Shanxi	158.57	45.70	5.29	6
Tianjin	172.40	44.77	5.01	6
Xinjiang Uygur	143.06	52.77	4.96	5
Yunnan	98.97	24.30	5.68	6
Zhejiang	91.61	31.48	5.21	6
Delhi	94.72	17.56	5.44	6
Himachal Pradesh	96.99	28.41	5.20	6
Haryana	87.10	17.97	5.00	6
Punjab	83.40	19.34	5.75	5
Uttaranchal	82.21	23.19	5.29	5
Adygey	123.78	39.11	5.21	6
Altay	169.18	63.26	5.94	5

Astrakhan'	180.43	48.05	5.25	6
Chechnya	128.96	41.08	5.43	6
Dagestan	102.64	40.73	5.86	6
Kabardin-Balkar	152.24	43.00	5.08	6
Krasnodar	123.84	39.13	5.21	6
Kalmyk	158.59	46.65	5.19	6
Orenburg	196.45	61.79	5.73	6
Rostov	139.83	46.80	5.89	6
Samara	179.97	57.77	5.89	6
Saratov	177.48	56.36	5.81	6
North Ossetia	104.21	41.63	5.94	6
Stavropol'	157.04	42.34	5.50	5
Volgograd	178.42	53.01	5.17	6
Alabama	72.53	29.80	5.83	4
Arkansas	100.03	35.55	5.68	6
Arizona	75.33	24.54	5.14	5
California	109.71	22.36	5.63	6
Colorado	157.16	45.08	5.24	6
Connecticut	150.39	40.49	5.23	5
Delaware	112.44	36.21	5.77	4
Georgia	100.79	29.87	5.40	6
Iowa	163.43	48.61	5.35	6
Idaho	157.30	42.44	5.51	5
Illinois	137.00	45.64	5.77	6
Indiana	133.00	43.23	5.60	6
Kansas	137.27	42.85	5.60	5
Kentucky	95.86	37.91	5.43	6
Louisiana	98.29	27.11	5.01	4
Massachussets	151.45	40.90	5.27	5
Maryland	95.12	37.50	5.39	6
Michigan	138.75	46.16	5.84	6
Minnesota	135.79	42.20199774	5.4588	5
Missouri	135.79	42.20	5.54	5
Mississippi	72.46	29.76	5.82	4
Montana	161.00	47.43	5.27	6
North Carolina	98.65	32.74	5.25	6
North Dakota	177.54	56.85	5.81	6
Nebraska	141.47	47.07	4.97	5
New Hampshire	135.60	44.95	5.71	6
New Jersey	97.75	38.90	5.54	6
New Mexico	125.71	36.96	5.48	4
Nevada	110.56	31.95	5.64	4
New York	151.88	41.06	5.28	5

Ohio	103.79	42.27	5.88	6
Oklahoma	123.33	37.12	5.03	5
Oregon	96.14	31.89	5.45	6
Pennsylvania	151.62	40.96	5.27	5
Rhode Island	125.99	40.22	5.30	6
South Carolina	107.15	30.57	5.47	4
South Dakota	174.22	51.02	5.05	6
Tennessee	120.92	35.15	5.28	4
Texas	112.52	27.16	4.89	4
Utah	158.19	45.53	5.28	6
Virginia	105.40	34.97	5.61	6
Washington	97.52	32.49	5.53	6
Wisconsin	171.55	49.79	5.97	5
West Virginia	123.56	38.96	5.20	6
Wyoming	163.12	48.39	5.34	6

Table S10. Application scenarios of specific countries and regions

Countries/regions	Average ambient temperature in winter/°C	Average ambient temperature in summer/°C	Share of heating days	Target user heating load/W	Target user cooling load/W
Afghanistan	5.10	24.32	0.53	1689.69	231.57
Albania	8.26	23.67	0.72	1374.10	167.09
Algeria	11.11	24.13	0.40	1088.80	213.22
Argentina	11.72	23.71	0.39	1027.58	170.97
Armenia	3.58	23.55	0.85	1842.35	154.89
Azerbaijan	6.87	24.49	0.65	1512.87	249.01
Bhutan	11.10	23.28	0.61	1089.82	128.14
Bosnia and Herzegovina	6.12	23.40	0.85	1588.03	139.71
Bulgaria	5.79	23.44	0.79	1620.73	144.11
Croatia	6.79	23.48	0.76	1521.37	148.20
Cyprus	12.58	25.84	0.50	941.79	383.93
Democratic People's Republic of Korea	2.50	23.74	0.77	1950.50	174.14
France	8.11	23.15	0.78	1388.66	115.08
Georgia	5.93	23.35	0.74	1606.82	134.67
Greece	10.08	24.31	0.60	1191.66	230.58
Hungary	5.66	23.82	0.86	1633.89	182.28
Iraq	10.84	30.69	0.35	1115.96	868.94
Islamic Republic of Iran	6.12	24.83	0.41	1588.36	283.15
Israel	12.86	24.58	0.42	914.16	257.55
Italy	8.76	23.52	0.64	1324.14	151.66
Japan	7.69	23.56	0.41	1431.42	156.50
Jordan	10.69	24.63	0.47	1131.10	262.65
Kazakhstan	-0.28	23.74	0.66	2228.01	173.56
Korea	5.31	24.16	0.68	1668.77	215.83
Kuwait	13.16	31.60	0.25	883.63	959.66
Kyrgyzstan	3.28	23.55	0.76	1871.93	155.30
Lebanon	10.31	23.81	0.58	1169.09	181.48
Malta	14.00	24.76	0.58	799.56	275.52
Mongolia	-3.25	23.06	0.74	2525.09	106.29
Montenegro	6.98	23.37	0.80	1502.23	137.46
Morocco	12.55	23.93	0.43	944.95	192.67
Nepal	10.93	23.99	0.44	1107.36	199.10
Norfolk Island	15.60	23.36	0.36	639.52	136.44
Peru	14.87	23.22	0.46	713.12	122.42

Plurinational State of Bolivia	12.81	23.54	0.51	918.96	153.80
Republic of Moldova	4.20	23.69	0.89	1779.84	168.72
Republic of North Macedonia	5.95	23.60	0.80	1604.61	159.86
Romania	4.92	23.42	0.79	1708.45	142.29
Serbia	5.89	24.05	0.84	1610.86	204.92
Slovenia	6.08	23.23	0.89	1592.15	122.52
Spain	10.67	23.81	0.62	1132.53	181.18
State of Palestine	12.11	24.94	0.46	988.81	293.58
Swaziland	13.75	23.80	0.40	825.45	179.54
Syrian Arab Republic	9.48	25.38	0.49	1251.76	337.91
Tajikistan	5.09	24.48	0.61	1691.32	248.37
Tunisia	12.31	24.80	0.44	968.74	279.67
Turkey	7.25	23.77	0.60	1474.85	176.98
Turkmenistan	6.17	26.35	0.53	1582.69	435.39
Ukraine	3.45	23.29	0.80	1854.58	128.51
Uruguay	12.01	23.79	0.56	998.51	178.54
Uzbekistan	5.49	25.50	0.56	1650.58	349.67

Table S11. Application scenarios of specific subnational states/ provinces/ autonomous regions

Subnational states/provinces/autonomous	Average ambient temperature in winter/°C	Average ambient temperature in summer/°C	Share of heating days	Target user heating load/W	Target user cooling load/W
New South Wales	12.44	23.36	0.47	955.97	136.11
South Australia	12.18	23.52	0.51	982.28	151.98
Rio Grande do Sul	12.63	24.00	0.39	936.64	199.70
Ontario	2.49	23.41	0.81	1950.63	140.85
Anhui	6.90	25.69	0.57	1510.08	369.05
Beijing	2.70	25.72	0.67	1929.91	372.18
Chongqing	9.64	25.61	0.56	1235.68	361.37
Fujian	11.17	25.50	0.42	1083.49	350.04
Gansu	3.48	23.14	0.74	1851.59	113.76
Guizhou	8.78	23.84	0.56	1321.80	183.69
Henan	6.20	25.55	0.60	1579.54	355.02
Hubei	7.83	25.83	0.56	1417.50	382.53
Hebei	3.42	25.17	0.62	1858.46	316.88
Heilongjiang	-4.10	23.67	0.82	2610.03	166.68
Hunan	8.69	26.21	0.51	1331.48	420.65
Jilin	-2.06	23.79	0.81	2405.73	179.12
Jiangsu	6.70	25.36	0.59	1530.14	336.05
Jiangxi	9.04	26.50	0.48	1295.82	450.02
Liaoning	0.77	23.99	0.73	2122.93	198.91
Nei Mongol	-1.62	23.43	0.70	2361.81	142.54
Ningxia Hui	2.65	23.82	0.80	1935.21	181.96
Sichuan	9.38	24.74	0.55	1261.75	273.75
Shandong	4.95	24.98	0.62	1704.65	298.50
Shanghai	8.08	26.17	0.62	1392.38	416.89
Shaanxi	5.43	24.31	0.66	1657.49	231.35
Shanxi	3.04	23.67	0.70	1896.17	166.80
Tianjin	3.44	25.59	0.65	1855.63	358.82
Xinjiang Uygur	1.25	24.16	0.62	2075.15	216.24
Yunnan	11.10	23.12	0.45	1090.19	112.04
Zhejiang	8.54	25.89	0.55	1345.81	388.55
Delhi	13.80	29.82	0.23	819.88	781.57
Himachal Pradesh	9.36	24.33	0.52	1263.80	232.69
Haryana	13.62	29.22	0.24	838.09	721.93
Punjab	12.99	28.72	0.28	900.75	671.65
Uttaranchal	11.46	24.92	0.41	1053.68	291.94
Adygey	5.40	24.28	0.83	1660.15	227.55
Altay	-2.30	23.57	0.90	2429.72	157.19

Astrakhan'	2.38	25.26	0.74	1962.43	325.87
Chechnya	4.57	23.86	0.76	1743.11	186.30
Dagestan	4.77	23.62	0.76	1723.02	161.83
Kabardin-Balkar	3.97	23.42	0.85	1803.13	141.50
Krasnodar	5.39	24.23	0.79	1661.08	222.59
Kalmyk	2.86	24.78	0.73	1913.99	277.89
Orenburg	-1.95	24.02	0.83	2394.77	202.02
Rostov	2.77	24.11	0.80	1923.47	210.52
Samara	-0.78	23.96	0.90	2278.30	196.36
Saratov	-0.35	23.84	0.83	2235.01	183.60
North Ossetia	4.45	23.25	0.86	1754.97	125.48
Stavropol'	4.10	23.79	0.76	1790.22	179.31
Volgograd	0.86	24.48	0.80	2113.69	247.91
Alabama	8.95	25.23	0.49	1304.95	322.67
Arkansas	7.13	25.69	0.56	1486.66	368.53
Arizona	11.16	27.88	0.41	1084.00	588.42
California	11.85	23.66	0.49	1014.83	165.81
Colorado	3.25	23.21	0.74	1875.24	121.09
Connecticut	4.88	24.41	0.84	1711.80	240.95
Delaware	6.27	25.18	0.73	1572.70	317.72
Georgia	8.81	24.83	0.51	1319.13	283.11
Iowa	2.13	24.59	0.74	1987.11	258.85
Idaho	4.06	23.89	0.78	1793.79	188.59
Illinois	3.24	24.33	0.69	1875.63	233.22
Indiana	3.91	24.40	0.70	1809.10	240.05
Kansas	4.65	25.64	0.64	1735.31	363.97
Kentucky	5.78	24.69	0.65	1621.92	268.82
Louisiana	10.13	25.78	0.39	1187.07	377.66
Massachussets	4.74	24.21	0.86	1726.20	220.92
Maryland	5.93	24.89	0.70	1607.18	289.37
Michigan	2.95	23.99	0.81	1905.15	198.88
Minnesota	0.36	24.20	0.82	2163.98	220.22
Missouri	4.87	25.17	0.64	1713.34	317.15
Mississippi	8.96	25.59	0.48	1303.52	359.27
Montana	2.50	23.45	0.83	1950.16	145.34
North Carolina	7.75	24.79	0.58	1424.87	279.36
North Dakota	-0.36	24.09	0.84	2236.05	208.81
Nebraska	2.80	24.98	0.71	1920.03	298.30
New Hampshire	3.48	24.28	0.89	1852.19	228.22
New Jersey	5.40	24.66	0.75	1659.73	266.47
New Mexico	6.33	23.94	0.61	1567.18	193.61
Nevada	8.47	26.71	0.53	1353.06	471.35
New York	4.68	24.12	0.79	1732.12	212.00

Ohio	4.17	24.16	0.74	1782.71	215.54
Oklahoma	6.68	26.31	0.56	1531.94	431.38
Oregon	7.83	23.17	0.79	1416.55	117.44
Pennsylvania	4.71	24.21	0.77	1728.54	220.60
Rhode Island	5.05	24.79	0.87	1695.23	278.65
South Carolina	8.94	25.22	0.53	1306.42	322.19
South Dakota	1.50	24.25	0.77	2050.24	225.48
Tennessee	7.02	24.95	0.61	1498.32	294.61
Texas	9.73	25.60	0.34	1227.19	359.92
Utah	3.10	23.54	0.69	1890.45	154.01
Virginia	6.63	24.81	0.65	1537.49	280.65
Washington	7.60	23.32	0.81	1439.85	131.70
Wisconsin	1.89	24.07	0.82	2010.68	207.46
West Virginia	5.43	23.92	0.74	1656.68	192.15
Wyoming	2.18	23.46	0.82	1982.36	146.11

Table S12. Properties of phase change materials in separate heat and cold storage systems

No.	Materials	Phase change temperature/°C	Latent heat/J·g⁻¹	Thermal conductivity /W·m⁻¹·K⁻¹	Specific heat capacity (l) /kJ·kg⁻¹·K⁻¹	Specific heat capacity (s) /kJ·kg⁻¹·K⁻¹	Density /kg·m⁻³	Cost /$·kg⁻¹	Reference
1	SA/CSS	65.9-66.4	186.1	0.33	2.18	2.18	580		[58]
2	SA	67-70.5	174.1-177.6	0.1255-0.1487	2.48	2.48	850		[58–60]
3	S72	72	155	0.58	2.13	2.13	1666	25.14*	[22]
4	Palmitic acid	62.5--64	185.4	0.162	2.8	1.9	886	2-150	[26,61]
5	Ice	0	210	2	4.2	2.06	992-1000		

Table S13. Time-of-use tariffs of four cities

Cities	Electricity price	
	On-peak price	Off-peak price
Arkansas	19.7 ¢/kWh (From Jun. to Oct.)	3.6 ¢/kWh
Beijing	1.2930 CNY/kWh	0.2939 CNY/kWh
Minnesota	16.73 ¢/kWh (From Jun. to Sept.)	7.79 ¢/kWh
Shanghai	0.617 CNY/kWh	0.2307 CNY/kWh

Reference

1. Gado, M. G. & Hassan, H. Energy-saving potential of compression heat pump using thermal energy storage of phase change materials for cooling and heating applications. *Energy* **263**, 126046 (2023).

2. Tay, N. H. S., Belusko, M. & Bruno, F. An effectiveness-NTU technique for characterising tube-in-tank phase change thermal energy storage systems. *Applied Energy* **91**, 309–319 (2012).

3. Lin, Y., Jia, Y., Alva, G. & Fang, G. Review on thermal conductivity enhancement, thermal properties and applications of phase change materials in thermal energy storage. *Renewable and Sustainable Energy Reviews* **82**, 2730–2742 (2018).

4. Cheng, W., Ding, M., Yuan, X. & Han, B.-C. Analysis of energy saving performance for household refrigerator with thermal storage of condenser and evaporator. *Energy Conversion and Management* **132**, 180–188 (2017).

5. Castell, A. *et al.* Natural convection heat transfer coefficients in phase change material (PCM) modules with external vertical fins. *Applied Thermal Engineering* **28**, 1676–1686 (2008).

6. Bergamini, R., Jensen, J. K. & Elmegaard, B. Thermodynamic competitiveness of high temperature vapor compression heat pumps for boiler substitution. *Energy* **182**, 110–121 (2019).

7. Zhao, B. & Wang, R. Thermal performance investigation of large-scale latent heat storage for heat supply. *Journal of Energy Storage* **56**, 106008 (2022).

8. Liu, Z. & Winterton, R. H. S. A general correlation for saturated and subcooled flow boiling in tubes and annuli, based on a nucleate pool boiling equation. *International Journal of Heat and Mass Transfer* **34**, 2759–2766 (1991).

9. Shah, M. M. A general correlation for heat transfer during film condensation inside pipes. *International Journal of Heat and Mass Transfer* **22**, 547–556 (1979).

10. Dong, Y., Yan, H. & Wang, R. Significant thermal upgrade via cascade high temperature heat pump with low GWP working fluids. *Renewable and Sustainable Energy Reviews* **190**, 114072 (2024).

11. Zhao, B. C., Li, T. X., He, F., Gao, J. C. & Wang, R. Z. Demonstration of Mg(NO3)2·6H2O-based composite phase change material for practical-scale medium-low temperature thermal energy storage. *Energy* **201**, 117711 (2020).

12. Zhao, B. C. & Wang, R. Z. A novel 3-D model of an industrial-scale tube-fin latent heat storage using salt hydrates with supercooling: A model validation. *Energy* **213**, 118852 (2020).

13. Yu, M., Zhang, C., Fan, Y., Zhang, X. & Zhao, Y. Performance study of phase change charging/discharging processes of condensing heat storage in cold regions based on a mathematical model. *Applied Thermal Engineering* **182**, 115805 (2021).

14. Du, R. Integrated heat pump with phase change materials for space heating. *Renewable and Sustainable Energy Reviews* (2024).

15. Kou, X. & Wang, R. Thermodynamic analysis of electric to thermal heating pathways coupled with thermal energy storage. *Energy* **284**, 129292 (2023).

16. Yang, L. *et al.* Shell-and-Tube Latent Heat Thermal Energy Storage Design Methodology with Material Selection, Storage Performance Evaluation, and Cost Minimization. *Applied Sciences* **11**, 4180 (2021).

17. Shan, L., Martin, A. & Chiu, J. N.-W. Techno-Economic Analysis of Latent Heat Thermal Energy Storage Integrated Heat Pump for Indoor Heating. in *36th International Conference on*

Efficiency, Cost, Optimization, Simulation and Environmental Impact of Energy Systems (ECOS 2023) 2265–2276 (ECOS 2023, Las Palmas De Gran Canaria, Spain, 2023). doi:10.52202/069564-0204.

18. Jaric, M., Martic, I., Budimir, N., Svetel, I. & Milanovic, M. Total costs of shell and tube heat exchangers with concentric helical tube coils. *Therm sci* **23**, 3661–3673 (2019).

19. Taal, M. Cost estimation and energy price forecasts for economic evaluation of retrofit projects. *Applied Thermal Engineering* **23**, 1819–1835 (2003).

20. Jiang, J., Hu, B., Ge, T. & Wang, R. Z. Comprehensive selection and assessment methodology of compression heat pump system. *Energy* **241**, 122831 (2022).

21. www.rubitherm.de.

22. epsltd.co.uk.

23. Kulish, V., Aslfattahi, N., Schmirler, M. & Sláma, P. New library of phase-change materials with their selection by the Rényi entropy method. *Sci Rep* **13**, 10446 (2023).

24. Reddy, K. S., Mudgal, V. & Mallick, T. K. Review of latent heat thermal energy storage for improved material stability and effective load management. *Journal of Energy Storage* **15**, 205–227 (2018).

25. Zhang, X. *et al.* Research Progress on the Phase Change Materials for Cold Thermal Energy Storage. *Energies* **14**, 8233 (2021).

26. Hirschey, J., Kumar, N., Turnaoglu, T. & Gluesenkamp, K. R. Review of Low-Cost Organic and Inorganic Phase Change Materials with Phase Change Temperature between 0°C and 65°C. in *International high performance buildings conference* (2021).

27. Faraji, M. Numerical study of the thermal behavior of a novel Composite PCM/concrete wall. *Energy Procedia* **139**, 105–110 (2017).

28. Zalba, B., Marín, J. M., Cabeza, L. F. & Mehling, H. Review on thermal energy storage with phase change: materials, heat transfer analysis and applications. *Applied Thermal Engineering* **23**, 251–283 (2003).

29. Kansara, K., Singh, V. K., Patel, R., Bhavsar, R. R. & Vora, A. P. Numerical investigations of phase change material (PCM) based thermal control module (TCM) under the influence of low gravity environment. *International Journal of Heat and Mass Transfer* **167**, 120811 (2021).

30. De Dios Cruz-Elvira, J. *et al.* A novel dodecanol/tepexil PCM composite for thermal energy storage in buildings. *Materials Chemistry and Physics* **284**, 126067 (2022).

31. Vicente, R. & Silva, T. Brick masonry walls with PCM macrocapsules: An experimental approach. *Applied Thermal Engineering* **67**, 24–34 (2014).

32. Koschenz, M. & Lehmann, B. Development of a thermally activated ceiling panel with PCM for application in lightweight and retrofitted buildings. *Energy and Buildings* **36**, 567–578 (2004).

33. Dixit, P. *et al.* Thermal Buffering Performance of a Propyl Palmitate/Expanded Perlite-Based Form-Stable Composite: Experiment and Numerical Modeling in a Building Model. *Energy Fuels* **35**, 2704–2716 (2021).

34. Biswas, K., Lu, J., Soroushian, P. & Shrestha, S. Combined experimental and numerical evaluation of a prototype nano-PCM enhanced wallboard. *Applied Energy* **131**, 517–529 (2014).

35. Zhao, D. & Tan, G. Numerical analysis of a shell-and-tube latent heat storage unit with fins for air-conditioning application. *Applied Energy* **138**, 381–392 (2015).

36. Li, Y., Zhou, J., Long, E. & Meng, X. Experimental study on thermal performance improvement

of building envelopes by integrating with phase change material in an intermittently heated room. *Sustainable Cities and Society* **38**, 607–615 (2018).

37. Guldentops, G. & Van Dessel, S. A numerical and experimental study of a cellular passive solar façade system for building thermal control. *Solar Energy* **149**, 102–113 (2017).

38. Kosny, J., Shukla, N. & Fallahi, A. *Cost Analysis of Simple Phase Change Material-Enhanced Building Envelopes in Southern U.S. Climates*. NREL/SR-5500-55553, DOE/GO-102013-3692, 1067934 http://www.osti.gov/servlets/purl/1067934/ (2013) doi:10.2172/1067934.

39. Zhu, N., Hu, N., Hu, P., Lei, F. & Li, S. Experiment study on thermal performance of building integrated with double layers shape-stabilized phase change material wallboard. *Energy* **167**, 1164–1180 (2019).

40. Iten, M., Liu, S. & Shukla, A. Experimental validation of an air-PCM storage unit comparing the effective heat capacity and enthalpy methods through CFD simulations. *Energy* **155**, 495–503 (2018).

41. Memarian, S., Kari, B. M., Fayaz, R. & Asadi, S. Single and combined phase change materials: Their effect on seasonal transition period. *Energy and Buildings* **169**, 453–472 (2018).

42. Wijesuriya, S., Brandt, M. & Tabares-Velasco, P. C. Parametric analysis of a residential building with phase change material (PCM)-enhanced drywall, precooling, and variable electric rates in a hot and dry climate. *Applied Energy* **222**, 497–514 (2018).

43. Castell, A., Martorell, I., Medrano, M., Pérez, G. & Cabeza, L. F. Experimental study of using PCM in brick constructive solutions for passive cooling. *Energy and Buildings* **42**, 534–540 (2010).

44. Leang, E., Tittelein, P., Zalewski, L. & Lassue, S. Numerical study of a composite Trombe solar wall integrating microencapsulated PCM. *Energy Procedia* **122**, 1009–1014 (2017).

45. Kong, X., Lu, S., Huang, J., Cai, Z. & Wei, S. Experimental research on the use of phase change materials in perforated brick rooms for cooling storage. *Energy and Buildings* **62**, 597–604 (2013).

46. Liu, C., Zhang, G., Arıcı, M., Bian, J. & Li, D. Thermal performance of non-ventilated multilayer glazing facades filled with phase change material. *Solar Energy* **177**, 464–470 (2019).

47. Huang, M. J., Eames, P. C. & Norton, B. Thermal regulation of building-integrated photovoltaics using phase change materials. *International Journal of Heat and Mass Transfer* **47**, 2715–2733 (2004).

48. Trp, A., Lenic, K. & Frankovic, B. Analysis of the influence of operating conditions and geometric parameters on heat transfer in water-paraffin shell-and-tube latent thermal energy storage unit. *Applied Thermal Engineering* **26**, 1830–1839 (2006).

49. Royon, L., Karim, L. & Bontemps, A. Thermal energy storage and release of a new component with PCM for integration in floors for thermal management of buildings. *Energy and Buildings* **63**, 29–35 (2013).

50. Ansuini, R., Larghetti, R., Giretti, A. & Lemma, M. Radiant floors integrated with PCM for indoor temperature control. *Energy and Buildings* **43**, 3019–3026 (2011).

51. Rady, M. Thermal performance of packed bed thermal energy storage units using multiple granular phase change composites. *Applied Energy* **86**, 2704–2720 (2009).

52. Liu, C. *et al.* Numerical analysis on thermal performance of a PCM-filled double glazing roof. *Energy and Buildings* **125**, 267–275 (2016).

53. Kant, K., Shukla, A. & Sharma, A. Heat transfer studies of building brick containing phase change materials. *Solar Energy* **155**, 1233–1242 (2017).

54. Zhou, G. & He, J. Thermal performance of a radiant floor heating system with different heat storage materials and heating pipes. *Applied Energy* **138**, 648–660 (2015).

55. Huang, K., Feng, G. & Zhang, J. Experimental and numerical study on phase change material floor in solar water heating system with a new design. *Solar Energy* **105**, 126–138 (2014).

56. Su, W., Darkwa, J. & Kokogiannakis, G. Review of solid–liquid phase change materials and their encapsulation technologies. *Renewable and Sustainable Energy Reviews* **48**, 373–391 (2015).

57. Agyenim, F., Hewitt, N., Eames, P. & Smyth, M. A review of materials, heat transfer and phase change problem formulation for latent heat thermal energy storage systems (LHTESS). *Renewable and Sustainable Energy Reviews* **14**, 615–628 (2010).

58. Wen, R., Zhang, W., Lv, Z., Huang, Z. & Gao, W. A novel composite Phase change material of Stearic Acid/Carbonized sunflower straw for thermal energy storage. *Materials Letters* **215**, 42–45 (2018).

59. Andiarto, R., Nuryadin, M. K., Taufik, A. & Saleh, R. Better latent heat and specific heat of stearic acid with magnetite/graphene nanocomposite addition for thermal storage application. *IOP Conf. Ser.: Mater. Sci. Eng.* **188**, 012049 (2017).

60. Zhu, C., Chen, Y., Cong, R., Ran, F. & Fang, G. Improved thermal properties of stearic acid/high density polyethylene/carbon fiber composite heat storage materials. *Solar Energy Materials and Solar Cells* **219**, 110782 (2021).

61. Zhou, D., Zhou, Y., Yuan, J. & Liu, Y. Palmitic Acid-Stearic Acid/Expanded Graphite as Form-Stable Composite Phase-Change Material for Latent Heat Thermal Energy Storage. *Journal of Nanomaterials* **2020**, 1–9 (2020).